WINTER STORM CONDITIONS LEADING TO EXCESSIVE RUNOFF ABOVE CALIFORNIA'S OROVILLE DAM DURING JANUARY AND FEBRUARY 2017

Allen B. White, Benjamin J. Moore, Daniel J. Gottas, and Paul J. Neiman

Record precipitation accompanied by high freezing levels and a damaged spillway caused California's Lake Oroville to overflow in February 2017, forcing a major evacuation.

This paper documents the record-setting precipitation (>2,500 mm) that fell in parts of California during the 2017 water year (1 October 2016–30 September 2017) and examines the hydrometeorological conditions leading up to and during an early February 10-day extreme precipitation

AFFILIATIONS: White, Gottas, and Neiman—NOAA/Earth System Research Laboratory/Physical Sciences Division, Boulder, Colorado; Moore—NOAA/Earth System Research Laboratory/Physical Sciences Division, and Cooperative Institute for Research in Environmental Sciences, University of Colorado Boulder, Boulder, Colorado

CORRESPONDING AUTHOR: Dr. Allen B. White, allen.b.white@noaa.gov

event when up to 690 mm of precipitation fell in the Feather River basin (FRB) along the western slope of the northern Sierra Nevada of California. A unique observing system developed by the National Oceanic and Atmospheric Administration's Physical Sciences Division (NOAA/PSD) for the California Department of Water Resources (CA-DWR; White et al. 2013) helps to elucidate the atmospheric and terrestrial conditions that caused this high-impact event, including how anomalously high freezing levels contributed to creating excessive runoff into Lake Oroville, at the bottom of the FRB. Uninterrupted operation of Oroville Dam's gated flood control spillway would have resulted in releasing enough water to keep the reservoir level below the emergency spillway (Fig. 1). However, damage to the flood control spillway suffered during the storm complicated dam operations, and a rapidly rising reservoir level eventually caused water to flow over the emergency spillway weir for the first time in the dam's history dating back to 1968.

California's Mediterranean climate is characterized by wet winters and dry summers. Precipitation falling during the winter wet season is responsible for filling reservoirs, moistening soils, and creating

FIG. 1. Oroville Dam and the two spillways used to mitigate excessive inflow into Lake Oroville during the early Feb 2017 extreme precipitation and runoff event. (Photo courtesy of the California Department of Water Resources.)

snowpack in the higher mountain regions. During the 2016 water year (WY2016), parts of Northern California received near normal precipitation, which allowed the state's two most voluminous reservoirs, Shasta Lake and Lake Oroville, to be filled above historical levels and to near capacity [current and historic precipitation and reservoir data are available from the California Data Exchange Center (CDEC); https://cdec.water.ca.gov/]. Meanwhile, a prolonged, record-breaking drought (Griffin and Anchukaitis 2014; Funk et al. 2014) continued in Southern California. During WY2017, much of California experienced record or near-record precipitation that remarkably filled all major reservoirs across California, ending the drought statewide (Boxall 2017). However, heavy precipitation events also caused major floods, mudslides, debris flows, and disruption to public life (Arsenault 2017). In addition, 188,000 people were evacuated from a region downstream of Oroville Dam because of concerns that erosion below the emergency spillway could lead to partial failure of the spillway weir.

Many of the storms that triggered flood-producing and/or reservoir-filling precipitation during WY2017 were the result of atmospheric rivers (ARs). ARs are long, narrow corridors of enhanced water vapor transport on the warm side of the polar cold front associated with extratropical cyclones (Ralph et al. 2004; Neiman et al. 2008; American Meteorological Society 2018). Composite images of integrated water vapor (IWV) derived from passive microwave observations from the Special Sensor Microwave Imager/Sounder (SSMIS) aboard polar-orbiting satellites (Wick et al. 2013) have been used to identify ARs (e.g., Neiman et al. 2008). In WY2017 there were 67 days when an AR intersected the California coast, triple the climatological average for the last 20 years comprising the satellite data era. Two consecutive ARs impacted the FRB above Oroville Dam during 2–11 February 2017, resulting in persistent heavy precipitation and excessive runoff into Lake Oroville.

2017 WATER-YEAR PRECIPITATION.

Figures 2a–c display 4-km gridded analyses of WY2017 accumulated precipitation (Fig. 2a) and accumulated precipitation percent of normal (Fig. 2b) from the National Weather Service Advanced Hydrologic Prediction Service (AHPS).
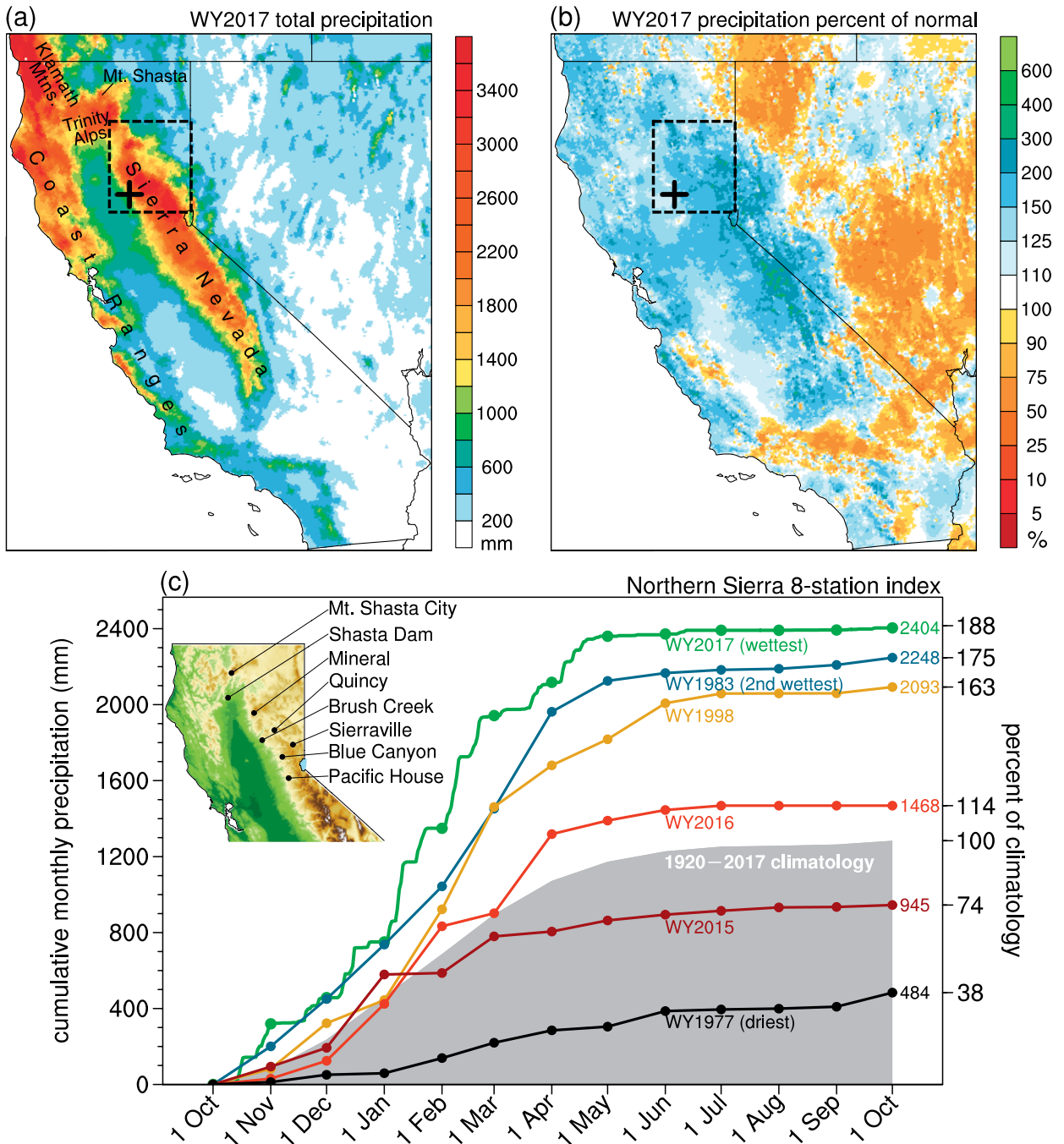
Fig. 2. NWS AHPS 4-km gridded analyses for WY2017: (a) accumulated precipitation (mm) and (b) accumulated precipitation percent of normal (%). The normal WY precipitation is derived from PRISM for 1981–2010. On each map, the black box outlines the domain shown in Fig. 3, and the plus sign marks the location of Oroville Dam. (c) Time series of the Northern Sierra precipitation eight-station index produced by CDEC for recent and notable water years. All time series are monthly except for the most recent WY, which is daily. The number to the right of each curve is the total WY precipitation (mm). The gray-shaded area represents the long-term average between 1920 and 2017. The inset map shows the locations of the eight stations composing the index, two of which are in the FRB at Quincy and Brush Creek.

For precipitation analyses over the western United States, AHPS uses a combination of gauges and the Parameter-Elevation Regressions on Independent Slopes Model (PRISM; Daly et al. 1994) to interpolate between gauges, especially in regions of complex terrain, where not many gauges exist. In most other parts of the United States, AHPS precipitation analyses are based on a combination of gauge,

radar, and satellite data, and a PRISM adjustment is not needed.

Many parts of the northern Sierra received more than 2,500 mm of precipitation (liquid equivalent) during WY2017. Other areas reaching this threshold include the Mount Shasta region and Trinity Alps at the northern terminus of the Central Valley, as well as the Klamath Mountains and Coast Ranges along the northwest California coast. The accumulated precipitation percent of normal, which is calculated with respect to the 1981–2010 climatology, demonstrates that most of the state received above-normal precipitation in WY2017, with only about the southern quarter of the state receiving near or below-normal precipitation (>75% of normal). The precipitation totals in much of the northern three-quarters of the state were >150% of normal, and in isolated regions of the Sierra the totals were >300% of normal.

Figure 2c shows time series of precipitation averaged over eight long-term rain gauge sites in the northern Sierra Nevada, which CDEC named the Northern Sierra eight-station index, for WY2017 and several other notable WYs. All time series are at monthly resolution except for WY2017, which is daily. WY2017 had the most precipitation on record for this index, which dates to 1920. The second and third wettest WYs were 1983 and 1998, respectively, both of which occurred during strong El Niño conditions over the Pacific. In contrast, the winter of WY2017 was characterized by weak La Niña conditions. The multivariate ENSO index (MEI; Wolter and Timlin 1993, 1998) provides a robust description of ENSO conditions. Positive MEI (El Niño) is generally associated with wetter WYs in the U.S. Southwest and drier WYs in the Northwest (e.g., Dettinger et al. 1998). The opposite is true for negative MEI (La Niña), which tends to be associated with drier WYs in the Southwest and wetter WYs in the Northwest (e.g., Redmond and Koch 1991). However, as indicated by Cayan et al. (1999), extreme precipitation and flooding in the California Sierra Nevada may be more common with La Niña. In 1983, 1998, and 2017, the mean MEI (December–March) values computed by averaging the three bimonthly MEI values (www.esrl.noaa.gov/psd/enso/mei/index.html) were 2.873, 2.662, and -0.583, respectively. Additional WYs with extreme precipitation will be required to fully understand the impacts of ENSO in this region.

The WY2017 precipitation was nearly twice the long-term average dating back to 1920 (gray-shaded area; Fig. 1c). More than one-half of this precipitation fell in January and February, the two wettest months of WY2017. Within this period there were several discrete multiday, heavy precipitation events. Early season (October–December) precipitation events during WY2017 moistened soils to near saturation and, in some cases, bolstered the snowpack (see "Storm impacts on the Feather River basin" section). These precursor conditions meant that later winter-season storms could potentially induce significant runoff given sufficiently warm temperatures. CDEC produces precipitation indices for other parts of the Sierra (not shown), although these do not date back as far as the Northern Sierra eight-station index. For example, for the Central Sierra five-station index during WY2017 ranked second behind WY1983. For the Southern Sierra (Tulare basin) six-station index, WY2017 ranked third behind WY1998 and WY1969.

SYNOPTIC-SCALE CONDITIONS FOR EARLY FEBRUARY 2017. The precipitation event over the FRB during 2–11 February 2017 involved two successive ARs on 2–3 and 5–11 February. The second AR formed and persisted in conjunction with three distinct pulses of enhanced water vapor transport in rapid succession linked to three successive low-level baroclinic disturbances, respectively, which included two mesoscale frontal waves and a strong cyclone (not shown). The key role of successive baroclinic disturbances in the persistence of ARs has been similarly documented in prior studies (e.g., Ralph et al. 2011; Sodemann and Stohl 2013; Neiman et al. 2016). Consistent with its persistence, the second AR culminated in greater (408 mm) precipitation at a selected gauge in the wettest part of the basin (Brush Creek; BRS) than the first AR (115 mm). For brevity, a snapshot of the synoptic conditions for only the second AR is provided in Fig. 3. A series of analogous maps for 1–12 February is available in the online supplement to this paper. The fields in Figs. 3b–d were derived from the NCEP Climate Forecast System (CFS), version 2 (Saha et al. 2014), analyses, obtained on a 0.5° × 0.5° grid. The anomalies in Figs. 3c and 3d were calculated relative to a smoothed daily 1979–2010 climatology, computed as in Bosart et al. (2017) using the NCEP Climate Forecast System Reanalysis (CFSR; Saha et al. 2010).

A composite image of SSMIS IWV during the afternoon of 7 February (Fig. 3a) depicts an AR with >30 mm of core water vapor intersecting the mid-California coast, including the San Francisco Bay area. This low-lying area creates a prominent gap in the coastal terrain that often allows the inland transport of water vapor, as discussed in White et al. (2015). At 850 hPa at 1200 UTC 7 February (Fig. 3b), the AR was embedded within a plume
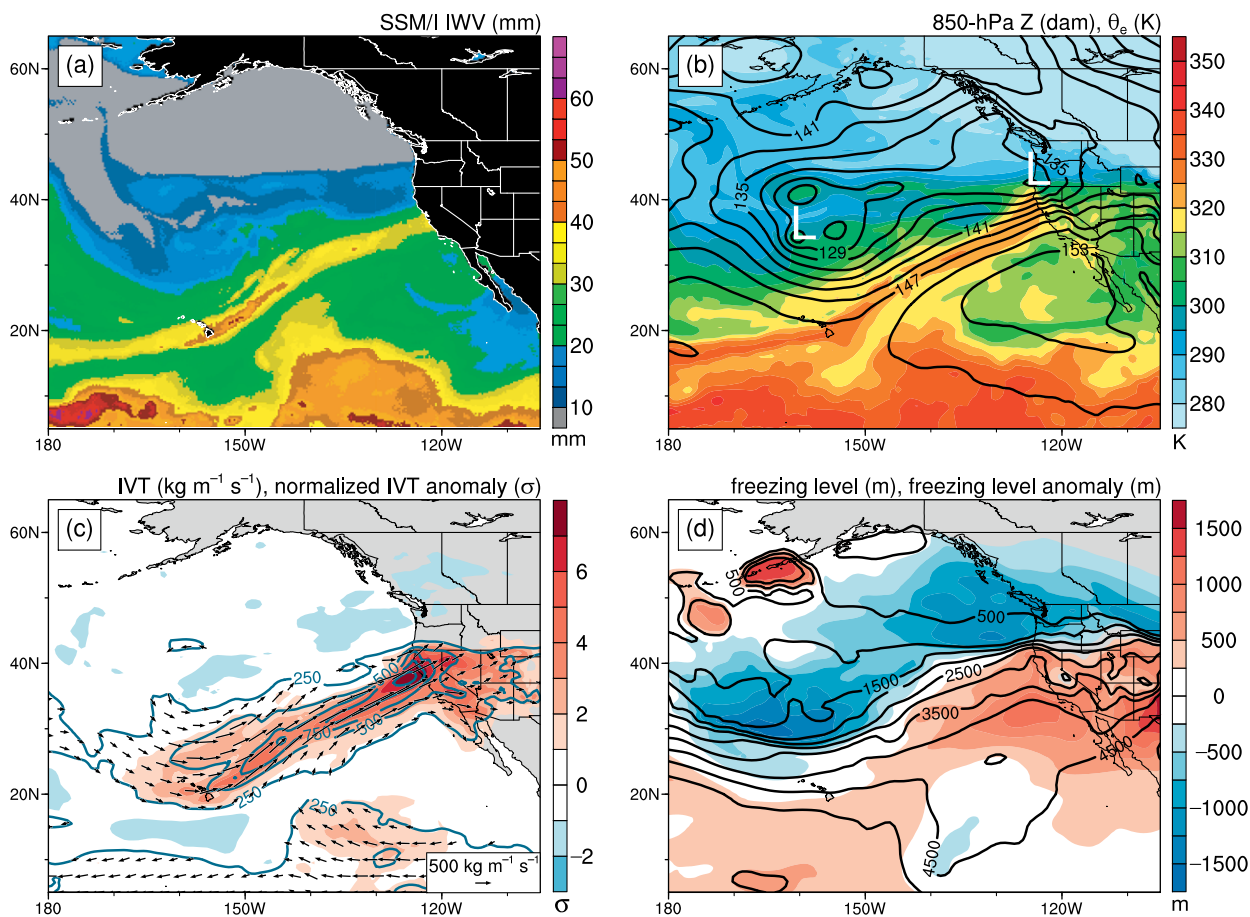
Fig. 3. Synoptic-scale conditions on 7 Feb 2017. (a) Composite SSMIS IWV (mm) from descending satellite orbits between 1200 and 2359 UTC 7 Feb. NCEP CFS, version 2, analyses for 1200 UTC 7 Feb: (b) 850-hPa geopotential height (dam; black contours) and equivalent potential temperature (K; color fill), (c) 1,000–300 hPa IVT (kg m^{-1} s^{-1}; blue contours; vector scale at bottom right) and normalized IVT anomaly (standard deviations; color fill), and (d) freezing level (m; black contours) and freezing-level anomaly (m; color fill). Anomalies are calculated with respect to the 1979–2010 climatology from the NCEP CFSR. The L symbols in (b) indicate the locations of baroclinic disturbances mentioned in the text.

of warm, moist air, reflected by high equivalent potential temperature values, aligned with inferred southwesterly confluent geostrophic flow. A large equivalent potential temperature gradient demarcating the poleward side of the plume signifies the presence of a polar cold front (Fig. 3b). The southwesterly flow, forced between an elongated area of low geopotential heights, comprising the latter two of the aforementioned baroclinic disturbances (L symbols in Fig. 3b), and an anticyclone to the southeast (Fig. 3b), favored the transport of water vapor from low and/or midlatitudes over the eastern North Pacific through the AR (not shown). The AR was consistently marked by an elongated corridor of anomalously strong 1,000–300-hPa vertically integrated water vapor transport (IVT; Fig. 3c) that

extended inland over California, featuring maximum IVT magnitude values of >1,000 kg m^{-1} s^{-1} and normalized anomalies in excess of six standard deviations. Over Northern California, freezing levels were generally in the 2,500–3,000-m range, and freezing-level anomalies were in the 500–1,000-m range (Fig. 3d), highlighting the warmth of the air mass in which the AR was embedded (Fig. 3b). A large freezing-level gradient was in place between the positive and negative anomalies over the eastern North Pacific and the Pacific Northwest, reflecting the polar cold front (Fig. 3d). In the ~5 days after 7 February (see maps in the online supplement), the final baroclinic disturbance underwent strong cyclogenesis and progressed northeastward, maintaining the AR extending into Northern California.

The persistent AR conditions corresponded to sustained warm, moist conditions and strong IVT (>500 kg m^{-1} s^{-1}) in the FRB.

The strength and persistence of the AR conditions during 2–11 February 2017 are hypothesized to have been critical for the occurrence of the high-impact precipitation in the FRB. To place the AR strength and persistence into climatological context, the CFS-based time-integrated IVT magnitude, an aggregate measure of IVT intensity and duration (Moore et al. 2012), averaged within a 1° × 1° box centered on Oroville Dam was analyzed for all 10-day periods during 1979–2017. This analysis revealed that 10-day periods encompassing the event in question (e.g., 0000 UTC 2 February–0000 UTC 12 February 2017) ranked near the top of the climatological distribution of the time-integrated IVT, exhibiting values at the ~99.8th percentile. This ranking was insensitive to moderate (±1 day) changes in the limits of the time integration. This result demonstrates the extraordinary strength and persistence of the AR conditions present during the early February 2017 event.

STORM IMPACTS ON THE FEATHER RIVER BASIN. *Feather River basin.* The Feather River above Lake Oroville drains about 932,400 ha and has five major tributaries. Four of these—West Branch, North Fork, Middle Fork, and South Fork—flow directly into Lake Oroville, and the fifth—the East Branch—is a tributary to the North Fork. Flows in the South and North Forks are managed for hydropower generation and there are numerous dams, reservoirs, penstocks, tunnels, and canals that transport or store water throughout the basin above Lake Oroville (Koczot et al. 2005). Altitudes range from 257 m at Oroville Dam to 2,903 m near Mount Lassen (see Fig. 4). Much of the basin lies at altitudes where temperatures can be either below or above freezing during the winter months. Thus, streamflow in the basin is highly dependent on both temperature and precipitation, in addition to other factors including dewpoint temperature, snowpack density, snowpack temperature, and precipitation type.

Figure 4 is a terrain elevation map of the FRB, with marked locations of the CA-DWR and cooperative agency rain gauges, cooperator snow sensors (with snow pillows), and a snow-level radar (SLR; Johnston et al. 2017) with a global positioning system-meteorology (GPS-Met) system at the base of Oroville Dam (OVL). Also shown in Fig. 4 are the locations of a radar wind profiler (RWP; Carter et al. 1995) at Chico, California (CCO), in the Sacramento Valley (Neiman et al. 2010) and a soil moisture observation site at Nevada City, California (NVC), in the neighboring Yuba River basin. Rain gauges also are located at OVL, CCO, and NVC. All of these instrumented sites are listed in Table 1. Snow pillows measure the water content of the snowpack based on the pressure created by the overlying mass of snow. The SLR measures the altitude (40-m vertical resolution) at which snow melts into rain (a.k.a. snow level) by detecting the altitude of the maximum radar reflectivity in the radar bright band (White et al. 2002). As defined here, the snow level exists below the freezing level, on average, by an altitude of 233 m based on comparisons between snow-level sensing radars and rawinsondes (White et al. 2010). GPS-Met provides a reliable method of measuring IWV with high temporal resolution under variable weather conditions (e.g., Gutman et al. 2004). Soil moisture is measured at depths of 10 and 15 cm using commercially available soil reflectometer probes (Zamora et al. 2011). The SLR, GPS-Met, and soil moisture probes are part of a large network of instruments installed across California to help CA-DWR and other end users monitor conditions that can lead to flooding and other hazardous weather impacts (White et al. 2013). The RWP at CCO derives the hourly averaged horizontal wind every 60 m in the vertical, and was part of the NOAA Hydrometeorology Testbed (HMT; hmt.noaa.gov) legacy observing network. In 2018, the RWP at CCO was removed in favor of a new RWP site established by CA-DWR and NOAA/PSD in October 2017 near the Thermalito power plant in Oroville, closer to the Oroville Dam (https://water.ca.gov/-/media/DWR-Website/Web-Pages/Library/Files/Publications/DWR/DWR-Magazines/2018/DWR-Magazine_Winter-2018_WEB_hyperlinks.pdf)

Soils in the midelevation ranges of the FRB have a high sand content and contain 8% clay based on the Soil Survey Geographic Database (Soil Survey Staff 2018). In the neighboring Yuba River basin at NVC (Fig. 4, Table 1), the clay content is 26%, allowing the soil at NVC to store more water than in the FRB. Therefore, we can use the soil moisture measurements from NVC to represent soil moisture evolution in the FRB, considering that soils in the FRB likely will saturate sooner than at NVC given equivalent precipitation. Soil moisture at NVC increased from its summer driest value of 13% volumetric water content (VWC) beginning with rainfall that occurred on 14 October 2016. Soils first reached field capacity (~41% VWC) at 15-cm depth on 30 October and remained within 10% of field capacity during January and February 2017. Wet soils contributed to the intense FRB runoff during the early February storm by not allowing most of the precipitation to be absorbed by the ground.
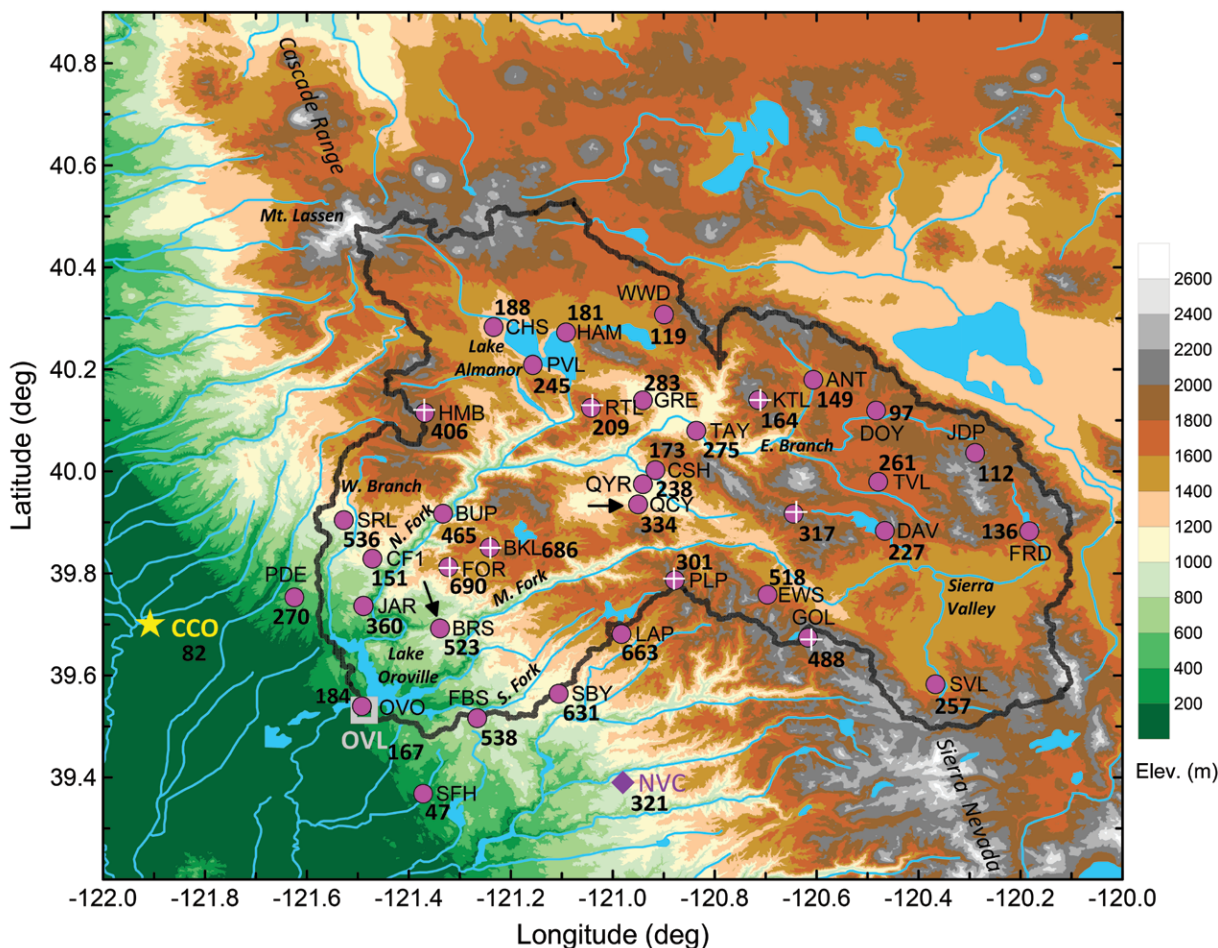
FIG. 4. Terrain elevation map of the FRB (dark gray outline) in Northern California with precipitation gauge locations (pink dots with three-letter site identifiers), cooperator snow sensor SWE sites (white plus signs), and precipitation totals (mm) for the 10-day period from 0000 UTC 2 Feb to 0000 UTC 12 Feb 2017 (boldface black text). The gauges at BRS and QCY highlighted with black arrows are two of the gauges in the eight-station index (see Fig. 1c). The SLR and GPS-Met instruments located at the base of OVL are denoted by the gray open square, the RWP at CCO is denoted by the yellow star, and the soil moisture observing site at NVC is denoted by the purple diamond. The watershed boundary was provided by the Center for Watershed Sciences at the University of California, Davis. Terrain and hydrography mapping datasets were provided by the U.S. Geological Survey. The precipitation data were provided by CDEC.

Orographic forcing of precipitation. The storm total precipitation (mm) from 0000 UTC 2 February to 0000 UTC 12 February 2017 for each rain gauge is plotted in boldface text in Fig. 4. The precipitation totals were derived from the hourly, and in a few cases, daily precipitation data provided by CDEC. The stations at Bucks Lake (BKL), Four Trees (FOR), La Porte (LAP), and Strawberry Valley (SBY) received the most precipitation (630–690 mm or 17%–18% of the water-year totals) and are all in the midelevation regions on the western side of the basin (~1,100–1,800 m) in a band above Lake Oroville. Less precipitation was observed at the central, eastern, and northern ends of the basin. The distribution of precipitation within the basin for this particular

storm is remarkably similar to the climatological distribution of precipitation [see Fig. 8 in Koczot et al. (2005)]. Therefore, recording the heaviest orographically enhanced precipitation near the reservoir as opposed to in other higher-elevation portions of the basin is not unusual. We selected three long-term measurement sites [Bucks Creek Powerhouse (BUP), Quincy (QCY), and SBY] within this midelevation region where orographic precipitation enhancement is favored climatologically to examine how this 10-day extreme precipitation event compared to other 10-day events. For this early February storm, the ranks of the 10-day precipitation totals for BUP (since 1959), QCY (since 1900), and SBY (since 1948) are in the ~99.4th, ~99.5th,

TABLE 1. Name, location, operating agency, and other details pertaining to the observing sites mapped in Fig. 4, ordered by site elevation. Sites highlighted in boldface received the greatest (>600 mm) total precipitation for the early Feb storm (see text). PG&E = Pacific Gas and Electric Company; CAL FIRE = California Department of Forestry and Fire Protection; USFS = U.S. Forest Service; CFA = Cal Fire Academy; RAWS = Remote Automated Weather System; SF PCU = San Francisco Public Utilities Commission.

Site ID	Site name	Lat (°)	Lon (°)	Elev (m)	Operational agency	Dataset(s) used	Storm total precipitation (mm)
CCO	Chico	39.70	−121.91	42	NOAA/PSD	Wind profiles	82
OVL	Oroville	39.53	−121.49	114	NOAA/PSD	Snow level, IWV	167
SFH	South Honcut Creek	39.37	−121.37	192	CA-DWR	Precipitation	47
ORO	Oroville Dam	39.54	−121.49	274	CA-DWR	Precipitation	184
PDE	Paradise	39.75	−121.62	533	CA-DWR	Precipitation	270
BUP	Bucks Creek Powerhouse	39.92	−121.33	536	PG&E	Precipitation	465
JAR	Jarbo Gap	39.74	−121.49	823	CAL FIRE	Precipitation	360
FBS	Forbestown	39.52	−121.27	866	PG&E	Precipitation	538
QCY	Quincy	39.94	−120.95	1,039	CA-DWR	Precipitation	334
NVC	Nevada City	39.39	−120.98	1,055	NOAA/PSD	Soil moisture	321
QYR	Quincy Ranger District	39.98	−120.94	1,067	USFS	Precipitation	238
SRL	Stirling City	39.90	−121.53	1,073	CA-DWR	Precipitation	536
TAY	Taylorsville	40.08	−120.84	1,079	CA-DWR	Precipitation	275
GRE	Greenville	40.14	−120.94	1,085	CA-DWR	Precipitation	283
BRS	Brush Creek	39.69	−121.34	1,085	CA-DWR	Precipitation	523
SBY	**Strawberry Valley**	**39.56**	**−121.11**	**1,161**	**CA-DWR**	**Precipitation**	**631**
CFI	CFA RAWS near Ione	39.83	−121.47	1,300	CAL FIRE	Precipitation	151
PVL	Prattville	40.21	−121.16	1,378	PG&E	Precipitation	245
CSH	Cashman	40.00	−120.92	1,378	National Park Service	Precipitation	173
CHS	Chester	40.28	−121.23	1,379	USFS	Precipitation	188
HAM	Hamilton Branch	40.27	−121.09	1,390	CA-DWR	Precipitation	181
ANT	Antelope Lake	40.18	−120.61	1,512	CA-DWR	Precipitation	149
SVL	Sierraville	39.58	−120.37	1,516	CA-DWR	Precipitation	257
LAP	**La Porte**	**39.68**	**−120.98**	**1,518**	**CA-DWR**	**Precipitation**	**663**
EWS	Plumas Eureka State Park	39.76	−120.70	1,557	CA-DWR	Precipitation	518
WWD	Westwood	40.31	−120.90	1,570	CAL FIRE	Precipitation	119
FOR	**Four Trees**	**39.81**	**−121.32**	**1,570**	**CA-DWR**	**Precipitation, SWE**	**690**
TVL	Thompson Valley	39.98	−120.48	1,647	CA-DWR	Precipitation	261
FRD	Frenchman Dam	39.88	−120.18	1,682	CA-DWR	Precipitation	136
DOY	Doyle Crossing	40.12	−120.48	1,728	CA-DWR	Precipitation	97
BKL	**Bucks Lake**	**39.85**	**−121.24**	**1,753**	**CA-DWR**	**Precipitation, SWE**	**686**
DAV	Lake Davis	39.88	−120.47	1,758	CA-DWR	Precipitation	227
RTL	Rattlesnake	40.13	−121.04	1,859	CA-DWR	Precipitation, SWE	209
HMB	Humbug	40.12	−121.37	1,981	CA-DWR	Precipitation, SWE	406
GOL	Gold Lake	39.67	−120.62	2,057	CA-DWR	Precipitation, SWE	488
PLP	Pilot Peak	39.79	−120.88	2,073	SF PUC	Precipitation, SWE	301
JDP	Jordan Peak	40.04	−120.29	2,076	CA-DWR	Precipitation	112
GRZ	Grizzly Ridge	39.92	−120.65	2,103	CA-DWR	Precipitation, SWE	317
KTL	Kettle Rock	40.14	−120.72	2,225	CA-DWR	Precipitation, SWE	164

and ~99.5th percentiles, respectively. Although the time-integrated IVT (see "Synoptic-scale conditions for early February 2017" section) and 10-day precipitation total climatologies use different historical periods, they both produce similarly high rankings. From these combined results, we conclude that the rapid succession of two ARs with embedded low-level baroclinic disturbances described in the section "Synoptic-scale conditions for early February 2017" was responsible for producing this extreme 10-day precipitation event.

The distribution of precipitation throughout the basin is largely attributed to orographically forced responses to the synoptic-scale kinematic
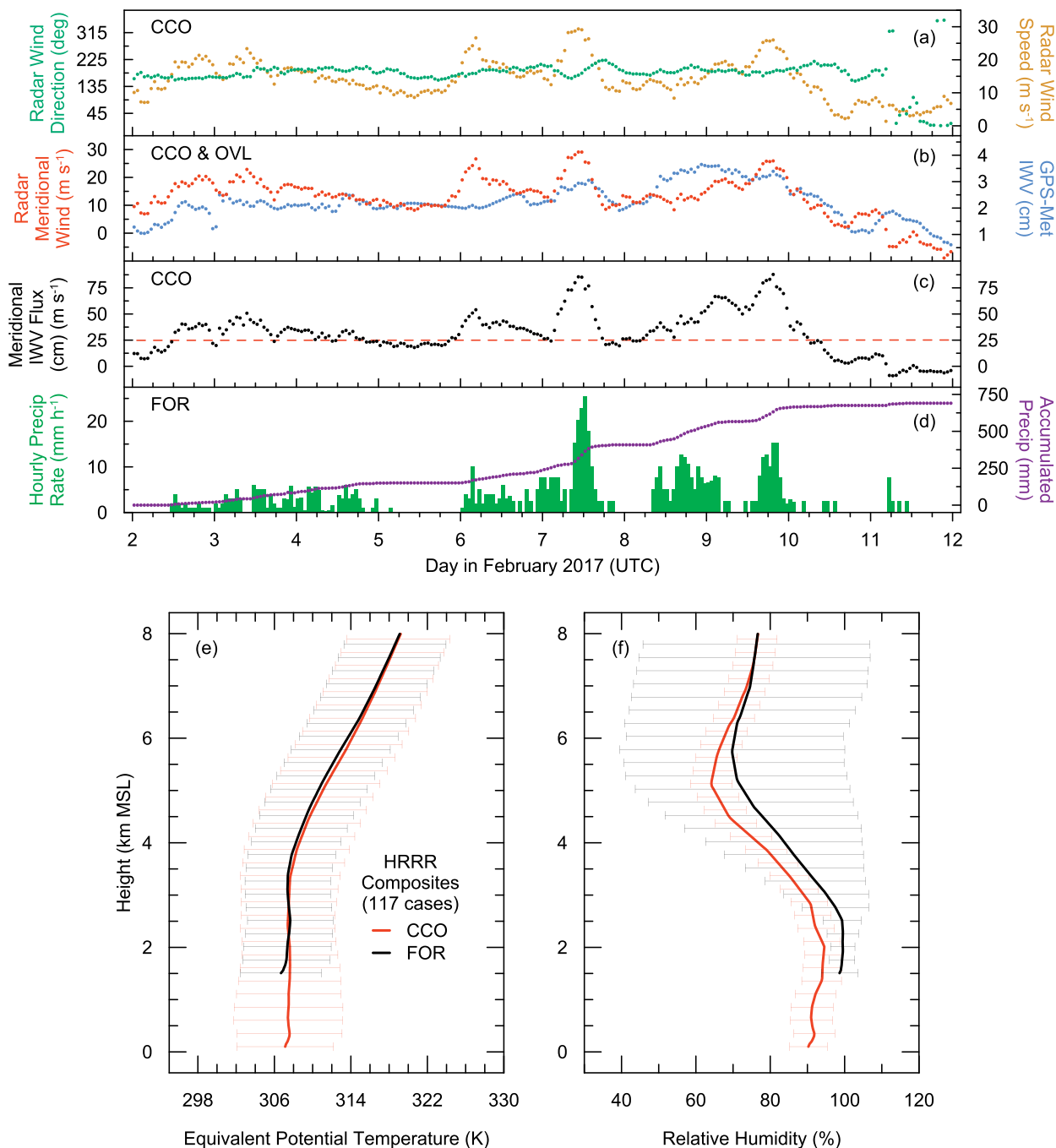
FIG. 5. (a) Horizontal wind direction (°; green dots) and horizontal wind speed (m s⁻¹; gold dots) averaged in the 0.75–1.25 km MSL layer, as measured by the RWP at CCO. (b) As in (a), but for radar-measured meridional wind (m s⁻¹; red dots) and IWV (cm; blue) from GPS-Met measurements at OVL. (c) Meridional IWV flux (cm m s⁻¹) computed from (b). Red dashed line drawn at 25 cm m s⁻¹ is used as a threshold to determine AR conditions (see text). (d) Hourly precipitation rate (mm h⁻¹; green bars) and accumulated precipitation (mm; purple dots) from precipitation gauge at FOR. (e) HRRR hourly composite average and standard deviation of equivalent potential temperature at CCO (red line and error bars) and FOR (black line and error bars) for 117 of the 139 h that received precipitation in (d) when HRRR grids were also available (see text). (f) As in (e), but for relative humidity (%).

and thermodynamic environment. Following Neiman et al. (2009), RWP measurements at CCO and GPS-Met measurements of IWV at OVL are used to investigate the upslope transport of water

vapor and the resulting enhancement of orographic precipitation (Figs. 5a–d). Owing to the predominant southerly flow during the storm (Fig. 5a) and the westward protrusion of the western slope

of the Sierra Nevada in the southwestern part of the FRB (Fig. 4), the low-level (i.e., 0.75–1.25 km MSL) northward-directed meridional flux of IWV (Fig. 5c) is moderately correlated with precipitation at FOR ($r = 0.6$ for IWV flux values greater than 25 cm m s^{-1}), similar to results found in Neiman et al. (2013, 2014) for the same region. This same IWV flux magnitude has been used as a minimum threshold for identifying AR conditions (Neiman et al. 2009). Based on Fig. 5c, AR conditions were present for 147 out of 240 h during the 10-day stormy period. Precipitation was measured at FOR during 139 h out of the 240 h and mostly for the same periods when AR conditions were present (Figs. 5c,d). Heavy precipitation (~10 mm h^{-1}) was measured during 18 of the 139 precipitating hours and only when AR conditions were present, a result first established by Neiman et al. (2009) for a coastal mountain site in Sonoma County, California, over four winter wet seasons.

The orographic response was likely further modulated by thermodynamic effects, as evidenced in composite vertical profiles of equivalent potential temperature and relative humidity from the NOAA operational High Resolution Rapid Refresh (HRRR; Benjamin et al. 2016) hourly initialization data at the times when precipitation occurred at FOR (Figs. 5e,f). Due to missing or incomplete model grids in the downloaded HRRR dataset, 22 of the 139 h that received precipitation are missing from the HRRR composite profiles. At FOR near-saturated conditions (relative humidity >95%) are present on average below ~3 km MSL (solid black line in Fig. 5f), and moist-static neutrality or instability was present between ~2.5 and ~3.5 km MSL, as indicted by either constant or decreasing equivalent potential temperature with height (solid black line in Fig. 5e). Similar conditions are noted in the HRRR over CCO. Thus, in the southwestern region of the basin, saturated maritime air parcels (with composite-average specific humidity values of ~6–8 g kg^{-1} below 1.5 km MSL; not shown) were uninhibitedly lifted along the lower western slope and then accelerated into convective updrafts (within the moist-unstable layer at ~2.5–3.5 km MSL) of sufficient depth to greatly enhance precipitation production.

Conversely, in the central, eastern, and northern ends of the basin, precipitation scavenging (e.g., downstream of heavily precipitating convective responses along the low to midelevations of the western slope) and rain-shadowing effects (e.g., downstream of the Sierra Crest along the southern border

of the eastern region of the basin, under southerly component flow regimes) likely acted to suppress precipitation accumulations. A 2-day (6–7 February 2017) loop of radar reflectivity scans in the vicinity of the FRB, as measured with the National Weather Service Weather Surveillance Radar-1988 Doppler (WSR-88D) radar at Davis, California (KDAX), is included in the online supplement. Here, regions of enhanced radar reflectivity (35–45 dBZ) associated with orographically induced convective precipitation elements anchored to the terrain above Lake Oroville are clearly evident along with transient precipitation regimes.

The aforementioned intensity and long duration of the precipitation contributed to making this storm so impactful. Another key factor resulting in intense runoff from this storm was the unusual warmth, as evidenced by the elevated freezing levels in Fig. 3d and by the SLR analysis described below, allowing a majority of the precipitation to fall as rain in the Feather River basin.

Snow-level impacts. We investigate the snow levels in the FRB quantitatively in Fig. 6a, which provides a time series of snow levels measured with the SLR at the base of Oroville Dam along with daily precipitation measured by the BRS gauge. Precipitation from the BRS gauge is chosen to be representative of the precipitation received in the climatologically wettest part of the basin, which was also the wettest part of the basin for the early February storm (Fig. 4). For context, time series span January–February 2017 to illustrate the unprecedented nature of the precipitation that fell during this period. A quote from CA-DWR's website on the Oroville spillways incident (https://water.ca.gov/What-We-Do/Emergency -Response/Oroville-Spillways/Background) underscores the significant hydrologic impact of the event: "January and February [2017] were the wettest in 110 years of Feather River hydrologic record. Lake Oroville received an entire year's average runoff of 4.4 million acre-feet in about 50 days during those two months." Figure 6b shows time series of this record inflow, outflow, and storage in Lake Oroville for the same 2-month period.

To investigate the climatological snow level in the FRB, we used the CFSR dataset ("Synoptic-scale conditions for early February 2017" section) to compute the 1979–2010 January–February mean freezing level during precipitation events. The mean freezing level was computed for all 6-h periods with precipitation exceeding three different thresholds corresponding to the 25th, 50th, and 75th percentiles, respectively, of
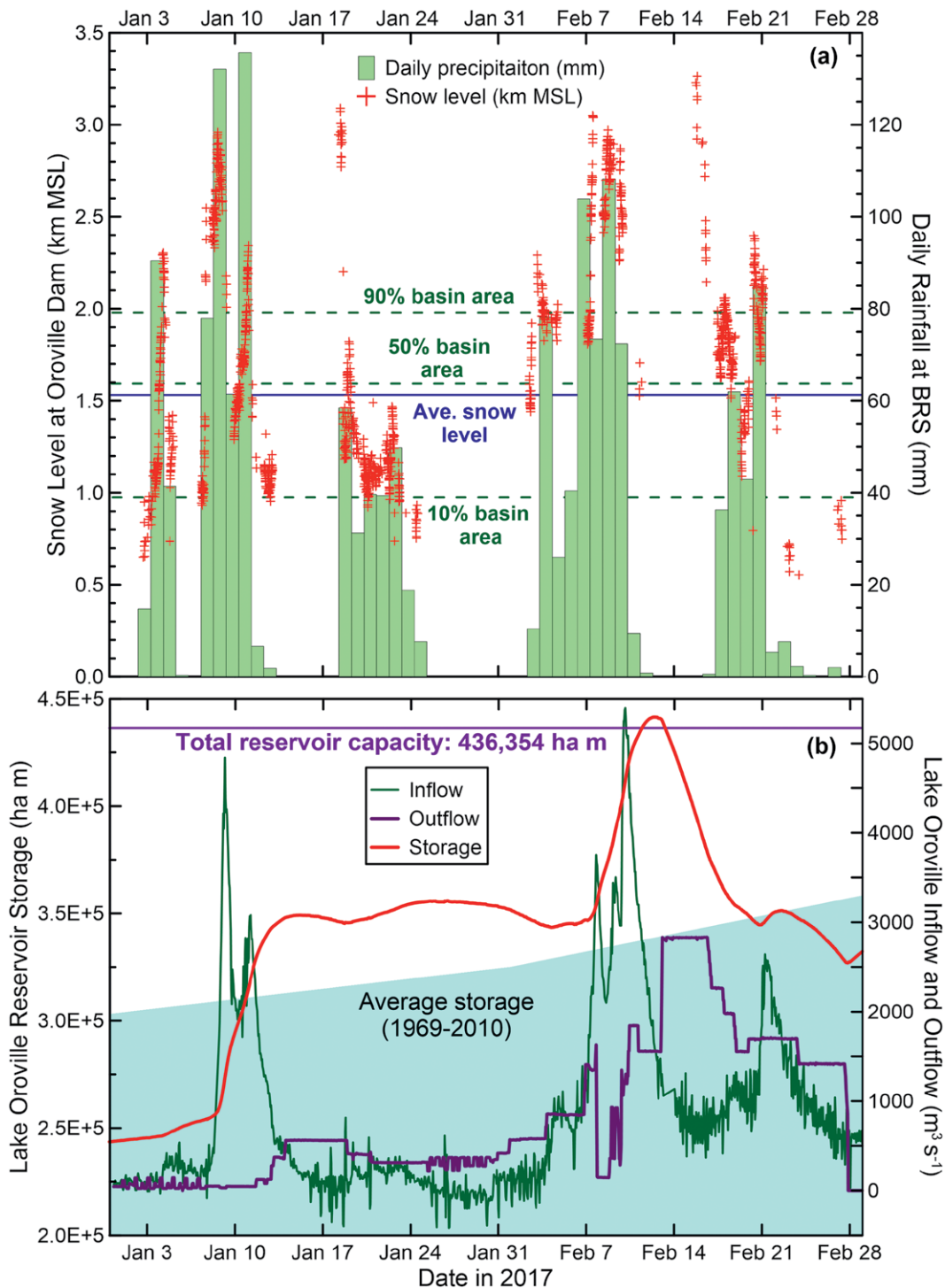
Fig. 6. (a) Daily accumulated precipitation (light green bars) from the gauge at BRS in the FRB for Jan and Feb 2017 along with snow levels (km MSL; red plus signs) observed by the SLR located at the base of Oroville Dam. Horizontal lines denote the average snow level in the watershed (solid blue line) and three basin-area elevation levels (percent of basin area; dashed dark green lines). (b) Hourly reservoir inflow (m³ s⁻¹; green curve), outflow (m³ s⁻¹; plum curve), and storage (ha m; red curve) in Lake Oroville during the same period as in (a), monthly average storage (cyan-shaded area), and reservoir capacity (purple horizontal line). Precipitation gauge and reservoir inflow, outflow, and storage data were acquired through CDEC.

the 1979–2010 January–February 6-h CFS precipitation climatology, excluding nonprecipitating periods, for a box encompassing the basin (39.5°–40.5°N, 120°–121.5°W). The mean freezing levels associated with the three precipitation thresholds were 1.805, 1.717, and 1.771 km, respectively. We averaged these and subtracted 233 m to arrive at a climatological snow level, 1.531 km, for direct comparison with SLR snow-level observations in Fig. 6a. Three basin-area elevation lines calculated using commercial contouring and surface mapping software are also indicated in Fig. 6a.

Snow levels observed during the early February storm were almost exclusively above the climatological snow level. Many of the heavier precipitation days in January and February had snow levels that were well above the 90% basin-area elevation level, suggesting that most of the precipitation on those days fell as rain. This is especially true for the second half of the early February storm. However, the substantive precipitation event in late January exhibited snow levels that were lower than climatology for most of the event. This event increased the midelevation basin snowpack until the early February storm ensued, when warm temperatures and rain on snow combined to increase the snowmelt and runoff. Table 2 lists several cooperator snow sensor sites in the basin where snow-water equivalent (SWE) is measured and compiled by the Natural Resources Conservation Service (NRCS). The locations of these sites are shown in Fig. 4 and other site details are listed in Table 1. The net SWE gained from 1 January to the date of maximum SWE before the rain-on-snow event

is indicated in addition to the reduction in SWE that occurred as a result of the rain-on-snow event. The largest reduction in SWE, 23.9 cm, occurred at FOR, which is in the part of the basin that also received the heaviest precipitation over the 10-day period (Fig. 4). If all of the lost SWE was converted to runoff, as opposed to densifying the snowpack, snowmelt would increase runoff at FOR by 35%. It is likely, therefore, that snowmelt throughout the basin, especially in the altitude range (~1,100–1,800 m) of the western part of the basin where the heaviest precipitation occurred, made a significant contribution to the overall runoff and excessive inflow to the reservoir, as discussed in the next section.

The snow level can sometimes dip when in areas of elevated terrain (Minder et al. 2011). Latent cooling from melting precipitation, adiabatic cooling from vertical motion, and the vertical distance associated with the melting process all contribute to this dip. Given the high snow levels observed during the early February storm, even a dip of several hundred meters in the snow level would not have changed the fact that there was significant runoff.

Reservoir operations. A summary of CA-DWR operations of the Oroville Dam in response to the extreme precipitation and extraordinary runoff that occurred in January and February 2017 follows. On 13 January, reservoir releases were increased from 249 m³ s⁻¹ (8,800 cfs) to 283 m³ s⁻¹ (20,000 cfs) to compensate for heavier inflow into the reservoir following a strong storm (8–13 January) that had particularly high snow levels on the two heaviest precipitation

TABLE 2. Cooperator snow sensor SWE (cm) and storm total precipitation (cm) measurements in the FRB from Jan to Feb 2017. SWE data were provided by NRCS. Precipitation data were provided by CDEC. Values in the far right column are assuming 100% of lost SWE is converted to runoff.

Site ID	Elev (m)	Net SWE gain from 1 Jan to date of max SWE prior to Feb rain-on-snow event (cm)	Date of max SWE prior to Feb rain-on-snow event	Storm total precip (cm)	SWE lost during Feb rain-on-snow event (cm)	Increase in potential runoff from lost SWE (%)
FOR	1,570	70.6	3 Feb	69.0	23.9	35
BKL	1,753	92.7	7 Feb	68.6	6.9	10
RTL	1,859	58.4	8 Feb	20.9	2.0	10
HMB	1,981	78.5	9 Feb	40.6	1.3	3
GOL	2,057	85.9	7 Feb	38.8	2.0	4
PLP	2,073	117.3	7 Feb	30.1	11.7	39
GRZ	2,103	66.8	7 Feb	31.7	4.3	14
KTL	2,225	71.4	7 Feb	16.4	14.0	85
Avg		80.2		39.5	8.3	21

days (Fig. 6a). During this storm event, reservoir inflow peaked at 4,839 m³ s⁻¹ (170,887 cfs) at 0500 UTC 9 January and remained above 2,832 m³ s⁻¹ (100,000 cfs) for 23 h on 8–11 January. Reservoir releases were increased to 1,416 m³ s⁻¹ (50,000 cfs) on 6 February but were curtailed temporarily on 7 February to allow time for engineers to inspect a sinkhole that had developed on the flood control spillway. However, as reservoir inflow and storage continued to increase sharply (Fig. 6b), reservoir releases were increased to 1,841 m³ s⁻¹ (65,000 cfs) on 10 February. During this prolonged storm event, reservoir inflow peaked at 5,393 m³ s⁻¹ (190,435 cfs) at 0300 UTC 10 February and remained above 2,832 m³ s⁻¹ (100,000 cfs) for 69 h on 7–11 February. At 1100 UTC 11 February, the reservoir storage exceeded capacity, causing water to flow over the emergency spillway weir. Erosion started to occur below the emergency spillway almost immediately. At 1100 UTC 12 February, the reservoir reached 275.1 m, the highest level ever recorded. In response, reservoir releases over the damaged flood control spillway were increased to 2,832 m³ s⁻¹ (100,000 cfs) to return the reservoir to a safer storage level while causing additional damage to the flood control spillway (a video produced by CA-DWR highlighting the flood control and emergency spillway releases on 12 February is available in the online supplement).

The evacuation of 188,000 residents living downstream of the dam was ordered at about 0000 UTC 13 February. The mandatory evacuation order was lifted on 14 February, but residents were warned that another evacuation could occur. During the remaining winter and until early 2019, major repairs were made to the flood control spillway, and the land beneath the emergency spillway was modified and reinforced to better accommodate runoff in case Lake Oroville ever exceeds its storage capacity again in the future. The design flow capacity of the gated flood control spillway is 7,646 m³ s⁻¹ (270,000 cfs). However, while repairs were being made, the operating flow capacity was set not to exceed 2,832 m³ s⁻¹ (100,000 cfs) for the period from November 2017 through January 2019. In September 2018, CA-DWR estimated the total cost for emergency response and reconstruction of the flood control and emergency spillways to be $1.1 billion.

SUMMARY. Highly anomalous precipitation in the winter of WY2017 ended a multiyear drought across California but also nearly caused a serious disaster with the Oroville Dam in early February 2017. Reservoir operations on Lake Oroville were hampered by a damaged flood control spillway, and excessive runoff during early February eventually caused the lake to flow over the dam's emergency spillway weir for the first time since the dam was installed in 1968. An emergency evacuation was ordered after it was determined that significant erosion below the emergency spillway could threaten the structural integrity of the spillway weir. However, it is important to keep in mind that if the flood control spillway had not been damaged, reservoir operators could have managed the inflow resulting from the early February storm using controlled releases.

Observations and meteorological analyses of this event revealed that intense and long-lived water vapor flux associated with two successive ARs supported heavy precipitation over the FRB during 2–11 February. The ARs were accompanied by anomalously warm conditions in Northern California, which elevated snow levels and exacerbated the flood threat by causing most of the precipitation to fall as rain instead of snow. The precipitation occurred in conjunction with strong orographic forcing as the water vapor flux associated with the ARs impinged on the northern Sierra. The combined intensity and persistence of the AR conditions and of the precipitation over the FRB during 2–11 February, as quantified by the 10-day time-integrated IVT and the 10-day accumulated precipitation, were extreme, ranking in the ~99.8th and ~99.5th percentiles, respectively, of the long-term climatology. The elevated snow levels and heavy precipitation promoted rapid and excessive runoff into Lake Oroville. This runoff was intensified by the presence of near-saturated soils and the partial melting of a preexisting snowpack established by several antecedent precipitation events during October–January. Future work will explore the synoptic- to planetary-scale atmospheric conditions that produced extreme precipitation in parts of California during WY2017 in the absence of El Niño forcing.

REFERENCES

American Meteorological Society, 2018: Atmospheric river. Glossary of Meteorology, http://glossary .ametsoc.org/wiki/Atmospheric_river.

Arsenault, K., 2017: Recent storms in California wreak havoc on infrastructure. *Emergency and Disaster Management Digest*, 27 February 2017, https://edmdigest .com/news/California-storms-wreak-havoc/.

Benjamin, S. G., and Coauthors, 2016: A North American hourly assimilation and model forecast cycle: The Rapid Refresh. *Mon. Wea. Rev.*, **144**, 1669–1694, https://doi.org/10.1175/MWR-D-15-0242.1.

Bosart, L. F., B. J. Moore, J. M. Cordeira, and H. M. Archambault, 2017: Interactions of North Pacific tropical, midlatitude, and polar disturbances resulting in linked extreme weather events over North America in October 2007. *Mon. Wea. Rev.*, **145**, 1245–1273, https://doi.org/10.1175/MWR-D-16-0230.1.

Boxall, B., 2017: Gov. Brown declares drought emergency is over. *LA Times*, 7 April 2017, www.latimes.com /local/lanow/la-me-brown-drought-20170407-story .html.

Carter, D. A., K. S. Gage, W. L. Ecklund, W. M. Angevine, P. E. Johnston, A. C. Riddle, J. Wilson, and C. R. Williams, 1995: Developments in UHF lower tropospheric wind profiling at NOAA's Aeronomy Laboratory. *Radio Sci.*, **30**, 977–1001, https://doi .org/10.1029/95RS00649.

Cayan, D. R., K. T. Redmond, and L. G. Riddle, 1999: ENSO and hydrologic extremes in the western United States. *J. Climate*, **12**, 2881–2893, https://doi .org/10.1175/1520-0442(1999)012<2881:EAHEIT >2.0.CO;2.

Daly, C., R. P. Neilson, and D. L. Phillips, 1994: A statistical–topographic model for mapping climatological precipitation over mountainous terrain. *J. Appl. Meteor.*, **33**, 140–158, https://doi.org/10.1175/1520 -0450(1994)033<0140:ASTMFM>2.0.CO;2.

Dettinger, M. D., D. R. Cayan, H. F. Diaz, and D. M. Meko, 1998: North–south precipitation patterns in western North America on interannual-to-decadal timescales. *J. Climate*, **11**, 3095–3111, https://doi .org/10.1175/1520-0442(1998)011<3095:NSPPIW >2.0.CO;2.

Funk, C., A. Hoell, and D. Stone, 2014: Examining the contribution of the observed global warming trend to the California droughts of 2012/13 and 2013/14. *Bull. Amer. Meteor. Soc.*, **95** (9), S11–S15.

Griffin, D., and K. J. Anchukaitis, 2014: How unusual is the 2012–2014 California drought? *Geophys. Res. Lett.*, **41**, 9017–9023, https://doi.org/10.1002 /2014GL062433.

Gutman, S. I., S. R. Sahm, S. G. Benjamin, B. E. Schwartz, K. L. Holub, J. Q. Stewart, and T. L. Smith, 2004: Rapid retrieval and assimilation of ground based GPS precipitable water observations at the NOAA Forecast Systems Laboratory: Impact on weather forecasts. *J. Meteor. Soc. Japan*, **82**, 351–360, https://doi.org/10.2151/jmsj.2004.351.

Johnston, P. E., J. R. Jordan, A. B. White, D. A. Carter, D. M. Costa, and T. E. Ayers, 2017: The NOAA FM-CW snow-level radar. *J. Atmos. Oceanic Technol.*, **34**, 249–267, https://doi.org/10.1175/JTECH-D-16-0063.1.

Koczot, K. M., A. E. Jeton, B. J. McGurk, and M. D. Dettinger, 2005: Precipitation-runoff processes in the Feather River basin, northeastern California, with prospects for streamflow predictability, water years 1971–97. U.S. Geological Survey Scientific Investigations Rep. 2004-5202, 82 pp.

Minder, J. R., D. R. Durran, and G. H. Roe, 2011: Mesoscale controls on the mountainside snow line. *J. Atmos. Sci.*, **68**, 2107–2127, https://doi.org/10.1175 /JAS-D-10-05006.1.

Moore, B. J., P. J. Neiman, F. M. Ralph, and F. Barthold, 2012: Physical processes associated with heavy flooding rainfall in Nashville, Tennessee, and vicinity during 1–2 May 2010: The role of an atmospheric river and mesoscale convective systems. *Mon. Wea. Rev.*, **140**, 358–378, https://doi.org/10.1175/MWR-D-11-00126.1.

Neiman, P. J., F. M. Ralph, G. A. Wick, J. D. Lundquist, and M. D. Dettinger, 2008: Meteorological characteristics and overland precipitation impacts of atmospheric rivers affecting the west coast of North America based on eight years of SSM/I satellite observations. *J. Hydrometeor.*, **9**, 22–47, https://doi .org/10.1175/2007JHM855.1.

——, A. B. White, F. M. Ralph, D. J. Gottas, and S. I. Gutman, 2009: A water vapour flux tool for precipitation forecasting. *Water Manage.*, **162**, 83–94, https:// doi.org/10.1680/wama.2009.162.2.83.

——, E. M. Sukovich, F. M. Ralph, and M. Hughes, 2010: A seven-year wind profiler–based climatology of the windward barrier jet along California's northern Sierra Nevada. *Mon. Wea. Rev.*, **138**, 1206–1233, https://doi.org/10.1175/2009MWR3170.1.

——, M. Hughes, B. J. Moore, F. M. Ralph, and E. M. Sukovich, 2013: Sierra barrier jets, atmospheric rivers, and precipitation characteristics in northern California: A composite perspective based on a network of wind profilers. *Mon. Wea. Rev.*, **141**, 4211–4233, https://doi.org/10.1175/MWR-D-13-00112.1.

——, F. M. Ralph, B. J. Moore, and R. J. Zamora, 2014: The regional influence of an intense Sierra barrier jet and landfalling atmospheric river on orographic precipitation in northern California: A case

study. *J. Hydrometeor.*, **15**, 1419–1439, https://doi
.org/10.1175/JHM-D-13-0183.1.

——, B. J. Moore, A. B. White, G. A. Wick, J. Aikins,
D. L. Jackson, J. R. Spackman, and F. M. Ralph,
2016: An airborne and ground-based study of a
long-lived and intense atmospheric river with me-
soscale frontal waves impacting California during
CalWater-2014. *Mon. Wea. Rev.*, **144**, 1115–1144,
https://doi.org/10.1175/MWR-D-15-0319.1.

Ralph, F. M., P. J. Neiman, and G. A. Wick, 2004:
Satellite and CALJET aircraft observations of at-
mospheric rivers over the eastern North Pacific
Ocean during the winter of 1997/98. *Mon. Wea. Rev.*,
132, 1721–1745, https://doi.org/10.1175/1520-0493
(2004)132<1721:SACAOO>2.0.CO;2.

——, ——, G. N. Kiladis, K. Weickmann, and D. M.
Reynolds, 2011: A multiscale observational case
study of a Pacific atmospheric river exhibiting
tropical–extratropical connections and a mesoscale
frontal wave. *Mon. Wea. Rev.*, **139**, 1169–1189, https://
doi.org/10.1175/2010MWR3596.1.

Redmond, K. T., and R. W. Koch, 1991: Surface climate
and streamflow variability in the western United
States and their relationship to large-scale circulation
indices. *Water Resour. Res.*, **27**, 2381–2399, https://doi
.org/10.1029/91WR00690.

Saha, S., and Coauthors, 2010: The NCEP Climate Fore-
cast System Reanalysis. *Bull. Amer. Meteor. Soc.*, **91**,
1015–1057, https://doi.org/10.1175/2010BAMS3001.1.

——, and Coauthors, 2014: The NCEP Climate Forecast
System version 2. *J. Climate*, **27**, 2185–2208, https://
doi.org/10.1175/JCLI-D-12-00823.1.

Sodemann, H., and A. Stohl, 2013: Moisture origin
and meridional transport in atmospheric rivers and
their association with multiple cyclones. *Mon. Wea.
Rev.*, **141**, 2850–2868, https://doi.org/10.1175/MWR
-D-12-00256.1.

Soil Survey Staff, 2018: Soil Survey Geographic
(SSURGO) Database. Natural Resources Conserva-
tion Service, U.S. Department of Agriculture, ac-
cessed 31 July 2018, https://sdmdataaccess.sc.egov
.usda.gov.

White, A. B., D. J. Gottas, E. T. Strem, F. M. Ralph,
and P. J. Neiman, 2002: An automated brightband
height detection algorithm for use with Doppler
radar spectral moments. *J. Atmos. Oceanic Tech-
nol.*, **19**, 687–697, https://doi.org/10.1175/1520-0426
(2002)019<0687:AABHDA>2.0.CO;2.

——, ——, A. F. Henkel, P. J. Neiman, F. M. Ralph,
and S. I. Gutman, 2010: Developing a performance
measure for snow-level forecasts. *J. Hydrometeor.*,
11, 739–753, https://doi.org/10.1175/2009JHM1181.1.

——, and Coauthors, 2013: A twenty-first-century Cali-
fornia observing network for monitoring extreme
weather events. *J. Atmos. Oceanic Technol.*, **30**, 1585–
1603, https://doi.org/10.1175/JTECH-D-12-00217.1.

——, P. J. Neiman, J. M. Creamean, T. Coleman, F. M.
Ralph, and K. A. Prather, 2015: The impacts of Cali-
fornia's San Francisco Bay Area gap on precipitation
observed in the Sierra Nevada during HMT and
CalWater. *J. Hydrometeor.*, **16**, 1048–1069, https://doi
.org/10.1175/JHM-D-14-0160.1.

Wick, G. A., P. J. Neiman, F. M. Ralph, and T. M.
Hamill, 2013: Evaluation of forecasts of the water
vapor signature of atmospheric rivers in opera-
tional numerical weather prediction models. *Wea.
Forecasting*, **28**, 1337–1352, https://doi.org/10.1175
/WAF-D-13-00025.1.

Wolter, K., and M. S. Timlin, 1993: Monitoring ENSO in
COADS with a seasonally adjusted principal compo-
nent index. *Proc. 17th Climate Diagnostics Workshop*,
Norman, OK, NOAA/NMC/CAC–NSSL–Oklahoma
Climatological Survey–CIMMS, School of Meteorol-
ogy, University of Oklahoma, 52–57.

——, and ——, 1998: Measuring the strength of ENSO
events: How does 1997/98 rank? *Weather*, **53**, 315–324,
https://doi.org/10.1002/j.1477-8696.1998.tb06408.x.

Zamora, R. J., F. M. Ralph, E. Clark, and T. Schneider,
2011: The NOAA Hydrometeorology Testbed
soil moisture observing networks: Design, in-
strumentation, and preliminary results. *J. Atmos.
Oceanic Technol.*, **28**, 1129–1140, https://doi.org
/10.1175/2010JTECHA1465.1.